

# Radar Positioning for Accurate Sensing of Pulse Waves at Multiple Sites Using a 3D Human Model

Takehito Koshisaka and Takuya Sakamoto, *Senior Member, IEEE*

**Abstract**—This study proposes a sensing method using a millimeter-wave array radar and a depth camera to measure pulse waves at multiple sites on the human body. Using a three-dimensional shape model of the target human body measured by the depth camera, the method identifies reflection sites on the body through electromagnetic scattering simulation. On the basis of the simulation, the radar system can be positioned at a suitable location for measuring pulse waves depending on the posture of the target person. Through measurements using radar and depth camera systems, we demonstrate that the proposed method can estimate the body displacement waveform caused by pulse waves accurately, improving the accuracy by 14% compared with a conventional approach without a depth camera. The proposed method can be a key to realizing an accurate and noncontact sensor for monitoring blood pressure.

**Index Terms**—Electromagnetic scattering, pulse wave, millimeter-wave radar, depth camera

## I. INTRODUCTION

**H**YPERTENSION increases the risk of cardiovascular diseases [1], and the percentage of hypertensive patients aged 30–79 years was 33.1% in 2019 [2]. Because regular blood pressure measurement is necessary to keep blood pressure within an appropriate range [3], it is necessary to have a sensing system for constant monitoring of blood pressure.

Blood pressure is related to pulse transit time, which is calculated from the arrival time of pulse waves measured at multiple sites on the human body [4]. This has been achieved mostly using contact sensors [5]–[7]. Research on noncontact pulse wave measurement has been conducted intensively to make the system unobtrusive and easy to set up; the use of millimeter-wave radar systems has been reported for such purposes [8]–[15]. For example, Oyamada *et al.* measured the body displacement waveform at the back and thigh simultaneously using a 79-GHz frequency-modulated continuous-wave (FMCW) radar system, and the accuracy was evaluated through simultaneous measurements with laser displacement sensors. To apply this technique in practice, we need to adjust the position of the radar system or the target person to receive echoes from the target sites on the body.

In this study, we propose a new approach for determining the position of the radar system depending on the target

person’s position and posture using electromagnetic scattering simulation to estimate which part of the body the reflected waves are received from. We reduce the computational complexity using a simplified approximation instead of full-wave electromagnetic simulation. Some studies on electromagnetic simulations with a human body are also based on the physical optics (PO) approximation because of its simplicity and practicality [17]–[22]. Some studies use geometrically simplified human models [23], [24], while other studies use precise human models obtained from a 3D laser scanner [25]–[27].

Konishi *et al.* reported electromagnetic wave scattering analysis with a human model obtained by a depth camera, assuming a radar frequency of 60 GHz, and visualized the reflection sites on the human body [28], [29]. Although the method proposed by Konishi *et al.* enables estimation of reflection sites on the human body surface, the method has not been applied to pulse wave measurement. In this study, we propose a method to achieve accurate pulse wave measurement without prior adjustment of the participant’s body posture by estimating the reflection sites on the target human body using electromagnetic wave scattering analysis to determine an appropriate radar position.

To obtain 3D human body shape data, Vahidpour and Sarabandi [27] used a 3D laser scanner to obtain a precise human model, which requires several cameras and a sufficiently large space. In this study, we use a depth camera to acquire a human model following the approach of Konishi *et al.* [28], [29]. Although some studies have used both a depth camera and a radar system [30], [31], they used the depth data only to estimate the position of the target person, whereas we consider the shape of the human body for radar measurement.

In this study, we propose a system to measure pulse waves at multiple locations with high accuracy by combining a depth camera and millimeter-wave radar. In Section II, we investigate the characteristics of millimeter-wave scattering from the human body surface by performing electromagnetic wave scattering analysis based on the PO approximation using a precise human model. In Section III, we propose a measurement system that integrates a depth camera and a millimeter-wave radar system, and evaluate its performance through experiments with two participants in the supine and prone positions.

Manuscript received April 16, 2023; revised May 31, 2024; accepted May 31, 2024. Date of publication May 31, 2024; date of current version May 31, 2024.

This work was supported in part by JST under Grants JPMJCE1307 and JPMJMI22J2, by SECOM Science and Technology Foundation, and JSPS KAKENHI under Grants 19H02155, 21H03427, and 23H01420.

T. Koshisaka and T. Sakamoto are with the Department of Electrical Engineering, Graduate School of Engineering, Kyoto University, Kyoto, Kyoto 615-8510, Japan (e-mail: sakamoto.takuya.8n@kyoto-u.ac.jp).

TABLE I  
PARAMETERS OF THE LASER SCANNER

Light source	Infrared
Repeatability	0.1 mm
Resolution	0.2 to 3 mm

## II. ELECTROMAGNETIC SCATTERING ANALYSIS AND ESTIMATION OF REFLECTION SITES

### A. Electromagnetic Scattering Analysis with the PO Approximation

The PO approximation is used for electromagnetic wave scattering analysis. This approximation calculates the current distribution on the target surface caused by the incident magnetic field and the normal vector of the surface. If the target material is modeled as a perfect electric conductor, the current density  $\mathbf{J}(\mathbf{r}')$  at position  $\mathbf{r}'$  on the target surface is approximated as

$$\mathbf{J}(\mathbf{r}') = 2\hat{\mathbf{n}}(\mathbf{r}') \times \mathbf{H}^{\text{inc}}(\mathbf{r}'), \quad (1)$$

where  $\hat{\mathbf{n}}(\mathbf{r}')$  is a unit normal vector, and  $\mathbf{H}^{\text{inc}}(\mathbf{r}')$  is an incident magnetic field.

Assuming that the polarization directions of the transmitting and receiving elements are both in the  $z$ -direction and the current density  $\mathbf{J}(\mathbf{r}')$  at each position  $\mathbf{r}'$  is approximated by an infinitesimal dipole, the  $z$ -component of the radiated electric field  $E_z(\mathbf{r}; \mathbf{r}')$  at antenna position  $\mathbf{r}$  is approximated as

$$E_z(\mathbf{r}; \mathbf{r}') = j \frac{kZ_0\ell}{4\pi|\mathbf{r} - \mathbf{r}'|} \hat{\mathbf{z}} \cdot \mathbf{J}(\mathbf{r}') e^{-jk|\mathbf{r} - \mathbf{r}'|}, \quad (2)$$

where  $\hat{\mathbf{z}}$  is a unit  $z$  vector,  $j$  is an imaginary unit,  $\ell$  is the length of the dipole,  $Z_0$  is the impedance of free space, and  $k$  is the wave number. Here we assume  $|\mathbf{r} - \mathbf{r}'|$  is sufficiently large compared with the reflection area.

Shijo *et al.* [32] proposed a PO-based method for visualizing high-frequency diffraction using a weighting function, called the eye function, defined as

$$w(\mathbf{r}; \mathbf{r}') = \begin{cases} \frac{1}{2} \left\{ \cos \left( \frac{\pi|\mathbf{r} - \mathbf{r}'|}{a_0} \right) + 1 \right\} & (|\mathbf{r} - \mathbf{r}'| \leq a_0) \\ 0 & (\text{otherwise}) \end{cases}, \quad (3)$$

where  $a_0$  is the radius of the eye function and should be sufficiently larger than the wavelength [32]. Using (3), we can approximate the intensity of the electric field received from the vicinity of the scattering point  $\mathbf{r}'$  as

$$E_{\text{scat}}(\mathbf{r}') = \left| \iint_{\Omega} w(\mathbf{r}; \mathbf{r}') E_z(\mathbf{r}; \mathbf{r}') dS \right|^2, \quad (4)$$

where  $\Omega$  is the entire target boundary surface.

A human 3D model is obtained using an iReal 2E laser scanner (SCANTECH Co., Ltd., Hangzhou, China), whose parameters are given in Table I. Fig. 1 shows  $E_{\text{scat}}(\mathbf{r}')$  for the human model in a supine position, where we set  $a_0 = 5\lambda$  and  $\lambda$  is the wavelength. In the figure, we see that reflection occurs mainly at several spots around the chest and abdomen. In addition, each area contributing reflection is small compared to the size of the human body.

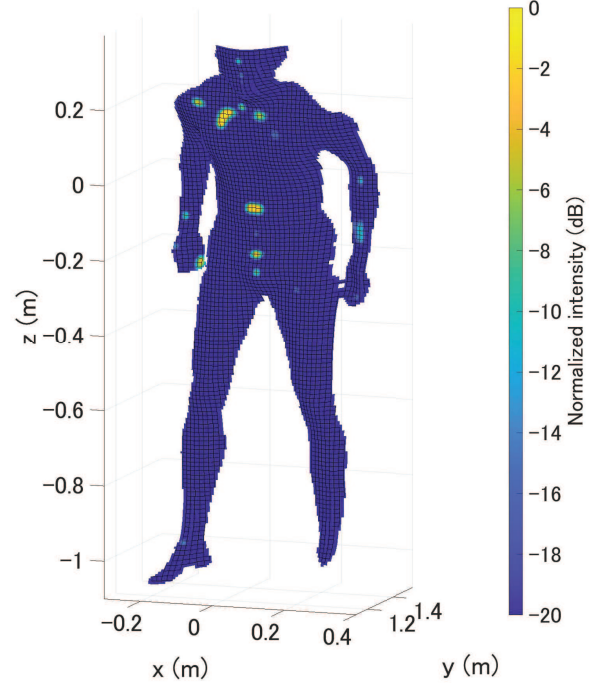


Fig. 1. Intensity of the reflected electric field distribution for a human model in a supine position calculated with PO for 79 GHz.

### B. Simplified Method for Estimation of Reflection Spots

Because the calculation of  $E_{\text{scat}}$  using the PO approximation according to Eq. (4) contains a double integral over an area much larger than the wavelength, the computational cost can be unacceptably large in practice. To address this issue, we introduce an even simpler method as follows: Let  $\mathbf{r}$  be a radar antenna position and  $\mathbf{r}'$  be a position on the target surface. We define

$$\xi(\mathbf{r}; \mathbf{r}') = \cos^{-1} \left( \frac{\hat{\mathbf{n}}(\mathbf{r}') \cdot (\mathbf{r} - \mathbf{r}')}{|\mathbf{r} - \mathbf{r}'|} \right), \quad (5)$$

where  $\xi$  is the angle between the radar line-of-sight direction and the normal vector  $\hat{\mathbf{n}}$ . Note that  $\xi$  satisfies  $0 \leq \xi \leq \pi$ .

If a point located at  $\mathbf{r}'$  on the target surface has a large  $|\xi|$ , the electric field scattered from the point is unlikely to contribute to the radar signal. Fig. 2 shows  $\cos \xi$  for a human model in a supine position with the same condition as in Fig. 1. Comparing this with Fig. 1, we see that  $\cos \xi$  is large close to the reflection area on the target surface, which indicates that  $\cos \xi$  can be used approximately to estimate the reflection areas instead of the PO approximation, and the computational cost in calculating  $\xi$  is much smaller than that of PO-based calculation.

## III. PROPOSED MEASUREMENT SYSTEM AND PERFORMANCE EVALUATION

### A. Experimental Setup

In this study, we propose a method to determine an appropriate location of the radar system to obtain echoes from target sites on the human body. The method assumes a system

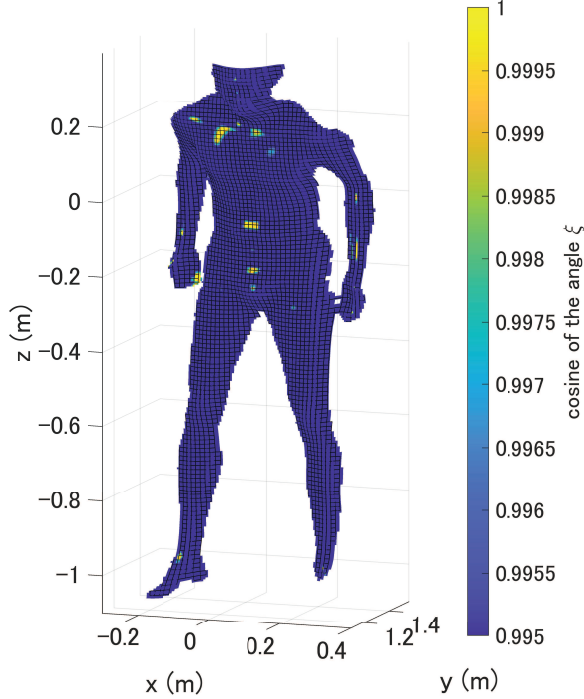


Fig. 2. Cosine of the angle between the radar line-of-sight vector and the normal vector.

with a millimeter-wave radar and depth camera installed over a target person lying in a prone position on a bed. We use an Intel RealSense D435 depth camera (Intel Corp., Santa Clara, California, U.S.) instead of the laser scanner used in the previous section. The parameters of the depth camera are given in Table II. Although the precision of a human model obtained with a depth camera is lower than that obtained with a laser scanner, a depth camera can acquire a human model in a shorter time and is suitable in practice.

Fig. 3 shows a diagram of the proposed measurement system with a coordinate system with the  $x$ -axis in the direction of the body axis and the  $y$ -axis vertical to the floor. The depth camera is fixed at the top of the bed and set as the origin of the coordinate system. The millimeter-wave radar can scan along the  $x$ -axis, where the  $x$ -axis is 1.1 m from the bed top.

The measurement procedure using the proposed method is as follows:

- 1) Obtain a human 3D model using a depth camera.
- 2) Visualize the radiated power distribution.
- 3) Locate the radar position to obtain echoes from the desired sites.
- 4) Measure a body displacement waveform using the radar

TABLE II  
PARAMETERS OF THE DEPTH CAMERA

Resolution	1280 × 720
Frame rate	30 fps
Horizontal field of view	87° ± 3°
Vertical field of view	58° ± 1°
Diagonal field of view	95° ± 1°

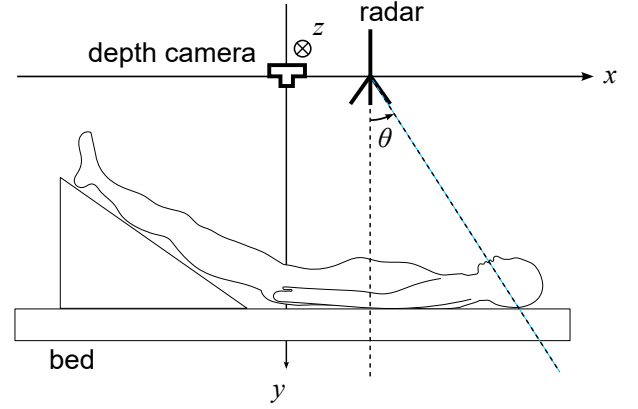


Fig. 3. Schematics of the proposed measurement system with a depth camera located at the origin and a radar system on the  $x$ -axis.

TABLE III  
PARAMETERS OF THE MILLIMETER-WAVE RADAR

Type of radar	FMCW radar
Center frequency	79.0 GHz
Bandwidth	3.4 GHz
Number of transmit antennas	3
Number of receive antennas	4
Spacing of transmit antennas	7.6 mm ( $2\lambda$ )
Spacing of receive antennas	1.9 mm ( $\lambda/2$ )
Beamwidth in the E-planes	±4°
Beamwidth in the H-planes	±35°
Range resolution	44 mm
Sampling frequency (slow-time)	145.6 Hz

system.

In this study, we used a radar module (T14\_01120112\_2D, S-Takaya Electronics Industry, Okayama, Japan) that comprises a single-chip millimeter-wave sensor (IWR 1443, Texas Instruments Inc., Dallas, Texas, United States). The parameters of the radar module are given in Table III. We used a multiple-input and multiple-output (MIMO) array radar. If the distance to a target from the radar antennas is sufficiently greater than the antenna aperture size, the array can be approximated as a virtual array with  $M = M_T M_R = 12$  elements, where  $M_T = 3$  and  $M_R = 4$  are the numbers of transmitting and receiving elements, respectively. The element spacing of the virtual array of the radar module was half the wavelength, and the angular resolution was approximately 8.5°. We used laser displacement sensors (CDX-150, OPEX FA Co., Ltd., Kyoto, Japan) as a reference for body displacement measurement. The parameters of the laser displacement sensors are shown in Table IV.

In this study, we developed software that displays an image of the human body with  $\cos \xi$  and indicates the intensity of

TABLE IV  
PARAMETERS OF THE LASER SENSOR

Measurement principle	triangulation
Wavelength of the light source	655 nm
Diameter of the spot size	120 $\mu$ m
Repeatability	0.2 $\mu$ m
Sampling frequency	200 Hz

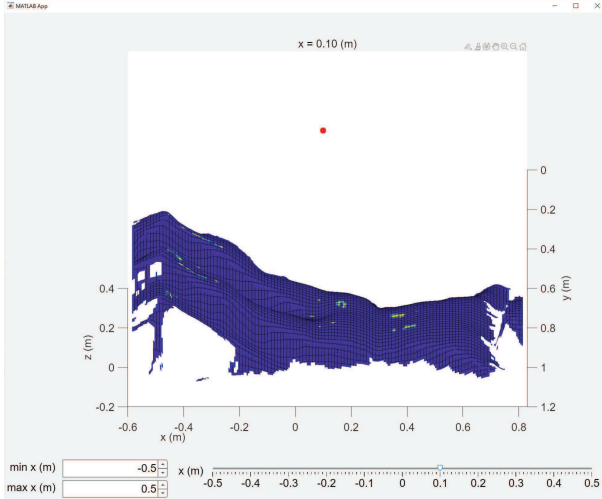


Fig. 4. Software for visualizing  $\cos \xi$  that indicates the intensity of the reflected electric field, where the red dot represents the position of a radar. Its  $x$ -coordinate can be changed with the slider.

the reflected electric field. With this software, the reflection sites on the body can be confirmed immediately when the radar position changes. The software runs on MATLAB as shown in Fig. 4, in which the image corresponds to  $\cos \xi(\mathbf{r})$  calculated using the simplified method in Section II-B. The  $x$ -coordinate of the radar position can be changed with the slider at the bottom of the screen. The radar position is expected to be optimized automatically if an appropriate objective function is defined. Despite this, the implementation of the optimization process is out of the scope of this study and will be an important topic to study in the future. In this study, we selected the radar position manually using this software.

### B. Array Radar Measurement of Pulse Waves

We propose a method for measuring a displacement waveform at multiple sites on the human body using a millimeter-wave radar system. Let us assume  $N$  reflections points on the target human body, and let  $\theta_n$  be the direction of arrival of the  $n$ th echo with the corresponding displacement  $d_n(t)$  for  $n = 1, 2, \dots, N$ . The  $n$ th echo is phase-modulated by the body motion as  $s_n(t) \propto e^{j2kd_n(t)}$ . For simplicity, we assume  $s_n(t) = e^{j2kd_n(t)}$  hereafter.

For a radar system with a virtual array comprising  $M$  elements with an element spacing of  $\lambda/2$ , the signal received from the  $m$ th element  $x_m(r, t)$  ( $m = 1, 2, \dots, M$ ) is expressed as a function of range  $r = c\tau/2$  and slow time  $t$ , where  $\tau$  is a fast time. The received signal  $x_m$  is then modeled as

$$x_m(r, t) = \sum_{n=1}^N a_{m,n}(r) s_n(t), \quad (6)$$

where  $a_{m,n}(r)$  is a complex constant corresponding to the propagation path between the  $n$ th target and  $m$ th antenna element. Then, we define signal vector  $\mathbf{x}(r, t) = [x_1(r, t), \dots, x_M(r, t)]^T$ , which is used to estimate the  $n$ th echo  $x_n(r, t)$  as  $\hat{x}_n(r, t) = \mathbf{w}_n^H \mathbf{x}(r, t)$  using an appropriate weight vector  $\mathbf{w}_n = [w_{1,n}, \dots, w_{M,n}]^T$  for the  $n$ th echo,

where superscripted  $T$  and  $H$  represent a transpose operator and a complex-conjugate transpose operator, respectively. By selecting range  $r_n$  for the  $n$ th echo, we can estimate the displacement  $d_n(t)$  as  $\hat{d}_n(t) = (1/2k) \angle \hat{x}_n(r_n, t)$ .

To determine weight vector  $\mathbf{w}$ , we use a minimum variance distortionless response (MVDR) method, which is also called directionally constrained minimization of power (DCMP) [33]. Let  $\mathbf{a}(\theta)$  be a steering vector for direction of arrival  $\theta$  expressed as  $\mathbf{a}(\theta) = [a_1(\theta), \dots, a_M(\theta)]^T$ , where  $a_m(\theta) = e^{jm\pi \sin \theta}$  for an array with antenna spacing  $\lambda/2$ .

The MVDR (DCMP) weight vector is determined by

$$\mathbf{w}(\theta) = (\mathbf{a}^H(\theta) R_{xx}^{-1} \mathbf{a}(\theta))^{-1} R_{xx}^{-1} \mathbf{a}(\theta), \quad (7)$$

where  $R_{xx}$  is a correlation matrix of  $\mathbf{x}$  formulated as  $R_{xx} = E[\mathbf{x}(r_n, t) \mathbf{x}^H(r_n, t)] \simeq (1/T) \int_0^T \mathbf{x}(r_n, t) \mathbf{x}^H(r_n, t) dt$  with the measurement time length  $T$ .

For example, when measuring the displacements at two sites  $(r, \theta) = (r_1, \theta_1)$  and  $(r_2, \theta_2)$  on the target body, we used the MVDR weight vectors  $\mathbf{w}(\theta_1)$  and  $\mathbf{w}(\theta_2)$  to estimate the displacements  $\hat{d}_1(t) = (1/2k) \angle \{\mathbf{w}^H(\theta_1) \mathbf{x}(r_1, t)\}$  and  $\hat{d}_2(t) = (1/2k) \angle \{\mathbf{w}^H(\theta_2) \mathbf{x}(r_2, t)\}$ .

### C. Experimental Evaluation of the Proposed Method

We performed experiments using a depth camera, a millimeter-wave radar system, and a pair of laser displacement sensors with two participants lying on a bed in supine and prone positions. The measurement was performed six times for each participant. For three out of the six times, the position of the radar system was adjusted using the proposed method (case A), and for the other three times, the position was not adjusted (case B). The radar position in case B was shifted by 0.3 m from the position in case A. The target sites on the body were selected to be the chest and the front of the thigh when the participants were in supine positions, and were selected to be the back and the back of the thigh when the participants were in prone positions. The radar and laser measurements were performed simultaneously for 30 s while the participants were holding their breaths to prevent respiratory effects.

The accuracy of the proposed method is evaluated in terms of the correlation coefficient  $\rho_n$  of the estimated and reference displacement waveforms  $\hat{d}_n(t)$  and  $d_n(t)$  defined as

$$\rho_n = \frac{1}{\hat{D}_n D_n} \int_0^T \hat{d}_n(t) d_n(t) dt, \quad (8)$$

where  $\hat{D}_n^2 = \int_0^T \hat{d}_n^2(t) dt$  and  $D_n^2 = \int_0^T d_n^2(t) dt$  assuming  $\int_0^T \hat{d}_n(t) dt = \int_0^T d_n(t) dt = 0$  for  $T = 5.0$  s.

We also evaluate the root-mean-square (RMS) error  $\varepsilon_n$  between  $\hat{d}_n(t)$  and  $d_n(t)$  defined as

$$\varepsilon_n^2 = \frac{1}{T} \int_0^T |\hat{d}_n(t) - \alpha d_n(t)|^2 dt \quad (9)$$

where  $\alpha$  is adjusted properly to compensate for the inclination of the laser displacement sensors. The range  $r_n$  for the measurement and definition of slow time  $t = 0$  are also adjusted to compensate for the imperfect synchronization of the radar and laser data.

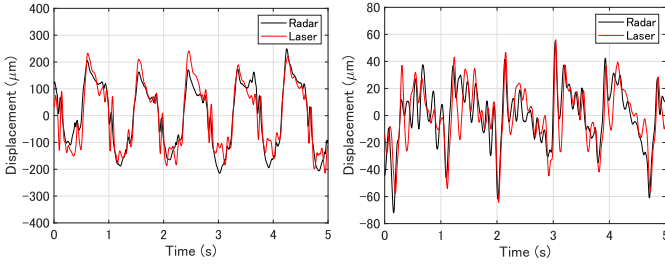


Fig. 5. Estimated and reference waveforms of the chest (left) and thigh (right) measured with a radar (black line) and a laser sensor (red line) for participant A in a supine position when the radar position is optimized.

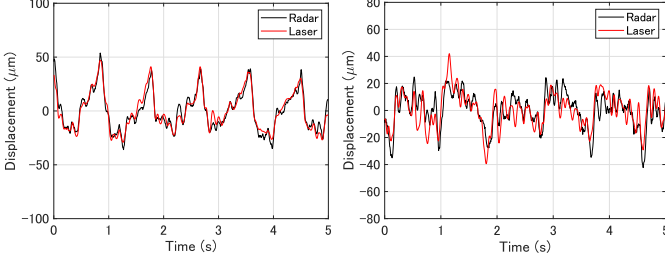


Fig. 6. Estimated and reference waveforms of the back (left) and thigh (right) measured with a radar (black line) and a laser sensor (red line) for participant A in a prone position when the radar position is optimized.

Figs. 5 and 6 show the estimated displacements when the radar position was adjusted using the proposed method for participant A in supine and prone positions, respectively. Here, the black and red lines represent the estimated and reference displacements, respectively. Figs. 7 and 8 show the estimated displacements when the radar position was shifted by 0.3 m from the case in Figs. 5 and 6.

First, Table V summarizes  $\rho_n$  and  $\varepsilon_n$  for six measurements of participant A in a supine position, where  $i = 1$  and 2 correspond to the chest and front of the thigh, respectively. The average correlation coefficients were 0.66 and 0.85 for the conventional and proposed methods, respectively. The average RMS errors were 26.3  $\mu\text{m}$  and 30.5  $\mu\text{m}$  for the conventional and proposed methods, respectively. Although the RMS error of the proposed method was 16% larger than that of the conventional method, the correlation coefficient of the proposed method was improved by 19% compared with that of the conventional method.

Next, Table VI summarizes results for participant B in a supine position. The average correlation coefficients were 0.56 and 0.87 for the conventional and proposed methods,

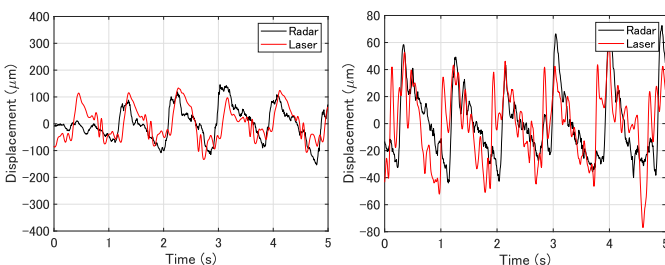


Fig. 7. Estimated and reference waveforms of the chest (left) and thigh (right) measured with a radar (black line) and a laser sensor (red line) for participant A in a supine position when the radar position is not optimized.

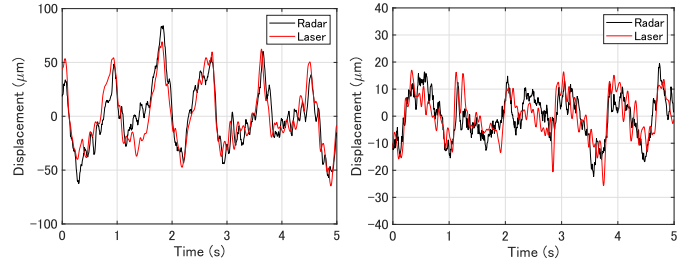


Fig. 8. Estimated and reference waveforms of the back (left) and thigh (right) measured with a radar (black line) and a laser sensor (red line) for participant A in a prone position when the radar position is not optimized.

TABLE V  
PERFORMANCE EVALUATION OF THE PROPOSED METHOD FOR PARTICIPANT A IN A SUPINE POSITION

Method	$\rho_1$	$\rho_2$	$\varepsilon_1$ ( $\mu\text{m}$ )	$\varepsilon_2$ ( $\mu\text{m}$ )
Conventional	0.58	0.57	56.0	24.5
	0.82	0.69	16.9	20.1
	0.51	0.80	21.4	18.8
Proposed	0.93	0.79	46.8	14.0
	0.82	0.71	77.3	16.3
	0.91	0.93	21.9	6.9

respectively. The average RMS errors were 52.3  $\mu\text{m}$  and 18.6  $\mu\text{m}$  for the conventional and proposed methods, respectively. The proposed method improved the correlation coefficient and RMS error by factors of 1.6 and 2.8, respectively.

Then, Table VII summarizes results for participant A in a prone position. The average correlation coefficients were 0.78 and 0.88 for the conventional and proposed methods, respectively. The average RMS errors were 14.2  $\mu\text{m}$  and 6.2  $\mu\text{m}$  for the conventional and proposed methods, respectively. The proposed method improved the correlation coefficient and RMS error by factors of 1.1 and 2.3, respectively.

Finally, Table VIII summarizes results for participant B in a prone position. The average correlation coefficients were 0.79 and 0.75 for the conventional and proposed methods, respectively. The average RMS errors were 15.3  $\mu\text{m}$  and 19.5  $\mu\text{m}$  for the conventional and proposed methods, respectively. In this case, the RMS error of the proposed method was worse than that of the conventional method by a factor of 1.3, whereas the correlation coefficient was improved by a factor of 1.1 using the proposed method. In this case, the estimation accuracy was degraded with the proposed method, partly owing to the significantly low accuracy in one of the six measurement datasets. If we exclude the last measurement, the average correlation coefficient and RMS error for the proposed method were 0.93 and 7.8  $\mu\text{m}$ , respectively.

TABLE VI  
PERFORMANCE EVALUATION OF THE PROPOSED METHOD FOR PARTICIPANT B IN A SUPINE POSITION.

Method	$r_1$	$r_2$	$e_1$ ( $\mu\text{m}$ )	$e_2$ ( $\mu\text{m}$ )
Conventional	0.74	0.42	51.3	23.7
	0.63	0.44	76.1	83.4
	0.61	0.54	54.9	24.2
Proposed	0.87	0.85	38.9	9.2
	0.97	0.80	16.1	13.9
	0.91	0.82	25.5	8.4

TABLE VII  
PERFORMANCE EVALUATION OF THE PROPOSED METHOD FOR PARTICIPANT A IN A PRONE POSITION.

Method	$\rho_1$	$\rho_2$	$\varepsilon_1$ ( $\mu\text{m}$ )	$\varepsilon_2$ ( $\mu\text{m}$ )
Conventional	0.88	0.70	14.2	6.2
	0.87	0.70	22.6	14.1
	0.88	0.63	13.8	14.7
Proposed	0.96	0.76	4.9	8.9
	0.97	0.80	4.1	8.8
	0.93	0.86	4.3	6.1

TABLE VIII  
PERFORMANCE EVALUATION OF THE PROPOSED METHOD FOR PARTICIPANT B IN A PRONE POSITION

Method	$\rho_1$	$\rho_2$	$\varepsilon_1$ ( $\mu\text{m}$ )	$\varepsilon_2$ ( $\mu\text{m}$ )
Conventional	0.94	0.52	11.9	10.0
	0.88	0.80	30.1	12.9
	0.93	0.67	8.8	17.8
Proposed	0.97	0.91	7.0	6.1
	0.96	0.87	7.2	10.7
	0.44	0.36	69.1	17.2

#### IV. CONCLUSION

In this study, we proposed a radar sensing system and method for measuring heart pulse waves at multiple sites on the human body using a depth camera and electromagnetic wave scattering analysis. To evaluate the performance of the proposed method, we conducted measurement involving two participants in supine and prone positions using both the proposed and conventional methods. The performances of the methods were evaluated in terms of the correlation coefficient and RMS error in estimating displacement waveforms using reference data taken with laser displacement sensors. Compared with the conventional method, the proposed method improved the estimation accuracy of the body displacement at two positions by 14% and 19% on average with respect to the correlation coefficient and RMS error, respectively. These results indicate that the proposed method can achieve accurate measurement of pulse waves at multiple sites. It will be important to study and develop a method for automatic optimization of the radar position using the proposed approach.

#### ETHICS DECLARATIONS

The experimental protocol involving human participants was approved by the Ethics Committee of the Graduate School of Engineering, Kyoto University (permit no. 201916). Informed consent was obtained from all human participants in the study.

#### REFERENCES

- [1] R. S. Vasan, M. G. Larson, E. P. Leip, J. C. Evans, C. J. O'Donnell, W. B. Kannel, and D. Levy, "Impact of high-normal blood pressure on the risk of cardiovascular disease," *N. Eng. J. Med.*, vol. 345, no. 18, pp. 1291–1297, Nov. 2001.
- [2] "World health statistics 2023: monitoring health for the SDGs, sustainable development goals," *World Health Organization*, 2023. [Online]. Available: <https://www.who.int/data/gho/publications/world-health-statistics>. Accessed on: May 8, 2024.
- [3] K. B. Bryant, J. P. Sheppard, N. Ruiz-Negrón, I. M. Kronish, V. Fontil, J. B. King, M. J. Pletcher, K. Bibbins-Domingo, A. E. Moran, R. J. McManus, and B. K. Bellows, "Impact of self-monitoring of blood pressure on processes of hypertension care and long-term blood pressure control," *J. Am. Heart Assoc.*, vol. 9, no. 15, Jul. 2020.
- [4] R. Mukkamala, J.-O. Hahn, O. T. Inan, L. K. Mestha, C.-S. Kim, H. Toreyin, and S. Kyal, "Toward ubiquitous blood pressure monitoring via pulse transit time: theory and practice," *IEEE Trans. Biomed. Eng.*, vol. 62, no. 8, pp. 1879–1901, Aug. 2015, DOI: 10.1109/TBME.2015.2441951.
- [5] P. C.-P. Chao, C.-C. Wu, D. H. Nguyen, B.-S. Nguyen, P.-C. Huang, and V.-H. Le, "The machine learnings leading the cuffless PPG blood pressure sensors into the next stage," *IEEE Sens. J.*, vol. 21, no. 11, pp. 12498–12510, Jun. 2021, DOI: 10.1109/JSEN.2021.3073850.
- [6] X. He, R. A. Goubran, and X. P. Liu, "Secondary peak detection of PPG signal for continuous cuffless arterial blood pressure measurement," *IEEE Trans. Instrum. Meas.*, vol. 63, no. 6, pp. 1431–1439, Jun. 2014, DOI: 10.1109/TIM.2014.2299524.
- [7] M. S. Roy, R. Gupta, and K. D. Sharma, "BePCon: A photoplethysmography-based quality-aware continuous beat-to-beat blood pressure measurement technique using deep learning," *IEEE Trans. Instrum. Meas.*, vol. 71, Oct. 2022, DOI: 10.1109/TIM.2022.3212750.
- [8] F. Michler, K. Shi, S. Schellenberger, T. Lenhard, F. Dassel, B. Scheiner, F. Lurz, R. Weigel, and A. Koelpin, "A radar-based vital sign sensing system for in-bed monitoring in clinical applications," in *Proc. 2020 German Microw. Conf. (GeMiC)*, Cottbus, Germany, 2020, pp. 188–191.
- [9] D. Buxi, J.-M. Redouté, and M. R. Yuce, "Blood pressure estimation using pulse transit time from bioimpedance and continuous wave radar," *IEEE Trans. Biomed. Eng.*, vol. 64, no. 4, pp. 917–927, Apr. 2017, DOI: 10.1109/TBME.2016.2582472.
- [10] M. P. Ebrahim, F. Heydari, T. Wu, K. Walker, K. Joe, J.-M. Redoute, and M. R. Yuce, "Blood pressure estimation using on-body continuous wave radar and photoplethysmogram in various posture and exercise conditions," *Sci. Rep.*, vol. 9, Nov. 2019, DOI: 10.1038/s41598-019-52710-8.
- [11] H. Zhao, X. Gu, H. Hong, Y. Li, X. Zhu, and C. Li, "Non-contact beat-to-beat blood pressure measurement using continuous wave Doppler radar," in *2018 IEEE/MTT-S Int. Microw. Symp. (IMS)*, Philadelphia, PA, USA, 2018, pp. 1413–1415.
- [12] J. E. Johnson, O. Shay, C. Kim, and C. Liao, "Wearable millimeter-wave device for contactless measurement of arterial pulses," *IEEE Trans. Biomed. Circuits Syst.*, vol. 13, no. 6, pp. 1525–1534, Dec. 2019, DOI: 10.1109/TBCAS.2019.2948581.
- [13] L. Lu, C. Li, and D. Y. C. Lie, "Experimental demonstration of noncontact pulse wave velocity monitoring using multiple Doppler radar sensors," in *Proc. 2010 Annual Int. Conf. IEEE Eng. Med. and Biol.*, Buenos Aires, Argentina, 2010, pp. 5010–5013.
- [14] F. Michler, K. Shi, S. Schellenberger, B. Scheiner, F. Lurz, R. Weigel, and A. Koelpin, "Pulse wave velocity detection using a 24 GHz six-port based Doppler radar," in *Proc. 2019 IEEE Radio Wireless Symp.*, Orlando, FL, USA, 2019.
- [15] Y. Oyamada, T. Koshisaka, and T. Sakamoto, "Experimental demonstration of accurate noncontact measurement of arterial pulse wave displacements using 79-GHz array radar," *IEEE Sens. J.*, vol. 21, no. 7, pp. 9128–9137, Apr. 2021, DOI: 10.1109/JSEN.2021.3052602.
- [16] Y. Oyamada, T. Koshisaka, G. Stankaitis, S. M. M. Islam, V. M. Lubecke, O. Borić-Lubecke, and T. Sakamoto, "Laser-based noncontact blood pressure estimation using human body displacement waveforms," in *Proc. 2022 IEEE/MTT-S Int. Microw. Symp. - IMS 2022*, Denver, CO, USA, 2022, pp. 1020–1022.
- [17] E. R. Ranjbar and M. Dehmollaian, "Scattering of an object with impedance surfaces using IPO and MLFMM," in *Proc. 2014 22nd Iranian Conf. Electr. Eng. (ICEE)*, Tehran, Iran, 2014, pp. 1610–1613.
- [18] E. R. Ranjbar and M. Dehmollaian, "Target above random rough surface scattering using a parallelized IPO accelerated by MLFMM," *IEEE Geosci. Remote Sens. Lett.*, vol. 12, no. 7, pp. 1481–1485, Jul. 2015, DOI: 10.1109/LGRS.2015.2409555.
- [19] A. Mazzinghi, L. Facheris, F. Cuccoli, and A. Freni, "2.5D physical optics based algorithm for vehicles classification through a FM-CW radar," in *Proc. 2018 15th European Radar Conf. (EuRAD)*, Madrid, Spain, 2018, pp. 257–260.
- [20] W. Zhang, H. Gomez-Sousa, J. Heredia-Juesas, and J. A. Martinez-Lorenzo, "Single-frequency imaging and material characterization using reconfigurable reflectarrays," *IEEE Trans. Microwave Theory Tech.*, vol. 69, no. 7, pp. 3360–3371, July 2021, DOI: 10.1109/TMTT.2021.3061597.
- [21] M. Arias, L. Perez-Eijo, Y. Rodriguez-Vaqueiro, B. Gonzalez-Valdes, J. Vázquez-Cabo, O. Rubiños-Lopez, A. Pino, and Y. Álvarez, "A physical optics simulator for dielectric bodies characterization using a multistatic radar," in *Proc. 2019 IEEE Int. Symp. Antennas Propag. and USNC-URSI Radio Sci. Mtg.*, Atlanta, GA, USA, 2019, pp. 819–820.

- [22] L. Corucci, E. Giusti, M. Martorella, and F. Berizzi, "Near field physical optics modelling for concealed weapon detection," *IEEE Trans. Antennas Propag.*, vol. 60, no. 12, pp.6052–6057, Dec. 2012, DOI: 10.1109/TAP.2012.2210017.
- [23] G. Manfredi, J.-P. Ovarlez, and L. Thirion-Lefevre, "Features extraction of the Doppler frequency signature of a human walking at 1 GHz," in *Proc. IGARSS 2019 - 2019 IEEE Intl. Geosci. and Remote Sens. Symp.*, Yokohama, Japan, 2019, pp. 2260–2263.
- [24] N. Keerativoranan, P. Hanpinitasak, K. Saito, and J.-I. Takada, "Analysis of non-intrusive hand trajectory tracking by utilizing micro-Doppler signature obtained from Wi-Fi channel state information," *IEEE Access*, vol. 8, pp. 176430–176444, Sept. 2020, DOI: 10.1109/ACCESS.2020.3026743.
- [25] L. Perez-Eijo, B. Gonzalez-Valdes, M. Arias, D. Tilves, Y. Rodriguez-Vaqueiro, O. Rubiños-López, A. Pino, F. García-Rial, and J. Grajal, "A physical optics simulator for multireflector THz imaging systems," *IEEE Trans. THz Sci. Technol.*, vol. 9, no. 5, pp. 476–483, Sept. 2019, DOI: 10.1109/THZ.2019.2930918.
- [26] F. Mokhtari-Koushyar and A. A. Shishegar, "Scattering analysis of human body modeled by NURBS surfaces in MM-wave band," in *Proc. 2014 Third Conf. Millimeter-Wave and THz Technol. (MMWATT)*, Tehran, Iran, 2014/2015.
- [27] M. Vahidpour and K. Sarabandi, "Millimeter-wave Doppler spectrum and polarimetric response of walking bodies," *IEEE Geosci. Remote Sens. Lett.*, vol. 50, no. 7, pp. 2866–2879, Jul. 2012, DOI: 10.1109/TGRS.2011.2176342.
- [28] K. Konishi and T. Sakamoto, "Automatic tracking of human body using millimeter-wave adaptive array radar for noncontact heart rate measurement," in *Proc. 2018 Asia-Pacific Microw. Conf.*, Kyoto, Japan, 2018, pp. 836–838.
- [29] T. Sakamoto, K. Konishi, K. Yamashita, M. Muragaki, S. Okumura, and T. Sato, "Adaptive array radar imaging of a human body for vital sign measurement," in *Proc. 2018 IEEE Int. Symp. Antennas Propag. & USNC/URSI National Radio Sci. Mtg.*, Boston, MA, USA, 2018, pp.617–618.
- [30] A. Shokouhmand, S. Eckstrom, B. Gholami, and N. Tavassolian, "Camera-augmented non-contact vital sign monitoring in real time," *IEEE Sens. J.*, vol. 22, no. 12, pp. 11965–11978, Jun. 2022, DOI: 10.1109/JSEN.2022.3172559.
- [31] I. V. Mikhelson, P. Lee, S. Bakhtiari, T. W. Elmer, A. K. Katsaggelos, and A. V. Sahakian, "Noncontact millimeter-wave real-time detection and tracking of heart rate on an ambulatory subject," *IEEE Trans. Inf. Technol. Biomed.*, vol. 16, no. 5, pp. 927–934, Sept. 2012, DOI: 10.1109/TITB.2012.2204760.
- [32] T. Shijo, T. Itoh, and M. Ando, "Visualization of high frequency diffraction based on physical optics," *IEICE Trans. Electron.*, vol. E87-C, no.9, pp.1607–1614, Sept. 2004.
- [33] K. Takao, M. Fujita, and T. Nishi, "An adaptive antenna array under directional constraint," *IEEE Trans. Antennas Propag.*, vol. 24, no. 5, pp. 662–669, Sept. 1976, DOI: 10.1109/TAP.1976.1141411.



**Takehito Koshisaka** received the B.E. degree in electrical and electronic engineering from Kyoto University, Kyoto, Japan, in 2021 and the M.E. degree in electrical engineering from the Graduate School of Engineering, Kyoto University, in 2023.



**Takuya Sakamoto** (Senior Member, IEEE) received a B.E. degree in electrical and electronic engineering from Kyoto University, Kyoto, Japan, in 2000 and M.I. and Ph.D. degrees in communications and computer engineering from the Graduate School of Informatics, Kyoto University, in 2002 and 2005, respectively.

From 2006 through 2015, he was an Assistant Professor at the Graduate School of Informatics, Kyoto University. From 2011 through 2013, he was also a Visiting Researcher at Delft University of Technology, Delft, the Netherlands. From 2015 until 2019, he was an Associate Professor at the Graduate School of Engineering, University of Hyogo, Himeji, Japan. In 2017, he was also a Visiting Scholar at University of Hawaii at Manoa, Honolulu, HI, USA. From 2019 until 2022, he was an Associate Professor at the Graduate School of Engineering, Kyoto University. From 2018 through 2022, he was also a PRESTO researcher of the Japan Science and Technology Agency, Japan. Since 2022, he has been a Professor at the Graduate School of Engineering, Kyoto University. His current research interests lie in wireless human sensing, radar signal processing, and radar measurement of physiological signals.

Prof. Sakamoto was a recipient of the Best Paper Award from the International Symposium on Antennas and Propagation (ISAP) in 2004; the Young Researcher's Award from the Information and Communication Engineers of Japan (IEICE) in 2007; the Best Presentation Award from the Institute of Electrical Engineers of Japan in 2007; the Best Paper Award from the ISAP in 2012; the Achievement Award from the IEICE Communications Society in 2015, 2018, and 2023; the Achievement Award from the IEICE Electronics Society in 2019; the Masao Horiba Award in 2016; the Best Presentation Award from the IEICE Technical Committee on Electronics Simulation Technology in 2022; the Telecom System Technology Award from the Telecommunications Advancement Foundation in 2022; and the Best Paper Award from the IEICE Communication Society in 2007 and 2023.